PHYSICAL REVIEW D **79,** 014004 (2009)

Number of QCD critical points with neutral color superconductivity

Zhao Zhang,[1,2,*] Kenji Fukushima,[1,†] and Teiji Kunihiro[2,‡]

[1]*Yukawa Institute for Theoretical Physics, Kyoto University, Kyoto 606-8502, Japan*

[2]*Department of Physics, Kyoto University, Kyoto 606-8502, Japan*

(Received 7 August 2008; published 7 January 2009)

We investigate the effect of the electric-charge neutrality in β equilibrium on the chiral phase transition by solving the chiral and diquark condensates in the two-flavor Nambu–Jona-Lasinio model. We demonstrate that the electric-charge neutrality plays a similar role as the repulsive vector interaction; they both weaken the first-order chiral phase transition in the high-density and low-temperature region. The first-order chiral phase transition is not affected, however, at finite temperatures where the diquark condensate melts. In this way the chiral phase transition could be second order at intermediate temperatures if the diquark effects overwhelm the chiral dynamics, while the first-order transition may survive at lower and higher temperatures. The number of the critical points appearing on the phase diagram can vary from zero to three, which depends on the relative strength of the chiral and diquark couplings. We systematically study the possibility of the phase structure with multiple QCD critical points and evaluate the Meissner screening mass to confirm that our conclusion is not overturned by chromomagnetic instability.

DOI: 10.1103/PhysRevD.79.014004 PACS numbers: 12.38.Aw, 11.10.Wx, 11.30.Rd, 12.38.Gc

I. INTRODUCTION

It is generally believed that quantum chromodynamics (QCD) exhibits a rich phase structure in an extreme environment such as high temperature and high baryon density. In the last decade the color-superconducting (CSC) phase has attracted lots of theoretical interest and triggered extensive studies of dense and cold quark matter [1–4]. At asymptotically high density that justifies the perturbative QCD calculations the color-flavor locked (CFL) phase [5] has been established as the ground state of quark matter. There, the pairing energy, the critical temperature, the screening properties, the collective excitation energy, and so on are well understood from the first-principle calculations.

In a practical sense, however, the accessible baryon density in nature would be, at most, ten times the normal nuclear density even in the interior of the compact stellar objects. In terms of the quark chemical potential the corresponding value should be less than 500 MeV in reality and thus other MeV energy scales such as the current and dynamical quark masses, the electric chemical potential, etc. take part into the dynamics. We are yet far from thorough understanding on the phase structure in this density region which is commonly referred to as the intermediate density. Going down from the CFL phase, we have to rely on chiral effective theories to unveil the possible CSC phases and to draw the boundary lines on the phase diagram which separate different CSC states [3,4].

Recently, an interesting proposal has been made for the plausible phase structure in the intermediate density region [6]. That is, there may exist a new QCD critical point (i.e. the terminal of the first-order phase boundary) induced by the $U_A(1)$-breaking vertex. This speculation is based on a general Ginzburg-Landau theory in terms of the order parameter fields constrained by QCD symmetries. There, the three-flavor anomaly term generates the coupling between $\langle \bar{\psi}\psi \rangle$ (chiral condensate), $\langle \psi\psi \rangle$ (diquark condensate), and $\langle \bar{\psi}\ \bar{\psi} \rangle$ (antidiquark condensate). It has been then argued that the resultant crossover of chiral restoration at small temperature embodies the hadron-quark continuity hypothesis [7]. Whether the new critical point appears with reasonable parameter set or not needs further investigation. Maybe, to settle the situation without ambiguity, we should wait for future developments in lattice QCD simulations at finite density.

In a different context, before discussed in Ref. [6], the appearance of another critical point at low temperature was pointed out in Ref. [8] within the two-flavor Nambu–Jona-Lasinio (NJL) model. The crucial ingredient in Ref. [8] is the four-fermion interaction in the vector channel as well as in the scalar one. In this case, the vector interaction diminishes the first-order chiral phase transition [9–11], which allows for enhanced competition between the chiral and diquark condensates in the widened coexisting phase. For some choices of the NJL model parameter two critical points show up along the phase boundary that signifies crossover, first-order transition, and crossover again with increasing temperature. We note that a similar phase diagram with two critical points is suggested in the lattice calculation of two-color QCD [12], though it seems to have not been established yet. As mentioned in Ref. [8], the vector-channel interaction could give a possible explanation for this two-color phase structure with two critical points.

*zhaozhang@pku.org.cn
†fuku@yukawa.kyoto-u.ac.jp
‡kunihiro@ruby.scphys.kyoto-u.ac.jp

In this paper we will reveal another mechanism leading to multiple QCD critical points; the electric-charge neutrality realized in β equilibrium can make chiral restoration being smooth cross over at low temperature, so that an analogous situation to Refs. [6,8] takes place. It is worth remarking here that imposing the electric neutrality has a similar effect on the thermodynamic potential to introducing the vector-channel interaction. One can understand this in terms of the electric chemical potential μ_e, which we define such that $\mu_e > 0$ not for positron but electron. In the model treatment without gauge fields a nonzero μ_e mimics the role of A_0 to neutralize the system. The point is that μ_e enters the dynamics like the vector-channel interaction; a vector-channel interaction $-G_{\rm V}(\bar{\psi}\gamma^\mu\psi)^2$ induces an effective (renormalized) chemical potential [9] which takes a form,

$$\mu_{\rm R} = \mu - 2G_{\rm V}\cdot\rho_q. \tag{1}$$

Here $G_{\rm V} > 0$ represents the repulsive vector coupling constant and ρ_q is the quark number density, $\langle\bar{\psi}\gamma^0\psi\rangle$. For two-flavor QCD μ_e leads to a mismatch between the u-quark chemical potential $\mu_u = \mu - \frac{2}{3}\mu_e$ and the d-quark one $\mu_d = \mu + \frac{1}{3}\mu_e$. We shall use a notation, $\bar{\mu}$, to denote the average chemical potential for u and d quarks resulting in

$$\bar{\mu} = \mu - \tfrac{1}{6}\mu_e. \tag{2}$$

Comparing the forms of $\mu_{\rm R}$ and $\bar{\mu}$ above, one may well anticipate that $\mu_e \neq 0$ can be taken in effect as a repulsive vector coupling for the bulk properties, in addition to keeping the electric neutrality. In physics terms, the electric chemical potential realizing a finite electric-charge density in part plays a role as a baryon chemical potential on its own. This situation is drastically different from the massless three-flavor case where the electric-charge generator happens to be traceless so that no coupling between the electric charge and baryon fluctuations arises (i.e. no term proportional to μ_e arises in $\bar{\mu}$ in this case).

To the best of our knowledge the direct coupling between the quark density and the electric chemical potential has drawn only little attention so far, though the vector-channel interaction and the electric neutrality have been investigated in separate contexts. In view of the results in Ref. [8], which is produced solely by the vector interaction, it is natural to expect that μ_e may also have a significant impact on both the chiral and CSC phase transitions.

The purpose of this paper is to investigate this issue seriously and depict an intuitive picture which opens a possibility to drive more QCD critical points than only one. We shall demonstrate our idea in the framework of the two-flavor NJL model for concreteness. Indeed, the competition between the chiral and diquark dynamics results in zero, one, two, and three critical points depending on the relative strength of the chiral and diquark couplings.

The paper is organized as follows. In Sec. II, the model is introduced and the formalism is presented. The numerical results and discussions are given in Sec. III. The final section is devoted to the summary and concluding remarks.

II. MODEL AND FORMALISM

We will explain the choice of the effective model, the model parameters, and the resulting thermodynamic potential in order. Since we adopt a standard description by the NJL model, the experts could skip to our results in Sec. III.

A. Model

Varieties of NJL-type models have been extensively used to investigate the CSC phase transition at moderate and large density [3] as well as at zero density [13,14]. For the two-flavor case, the commonly used Lagrangian of the NJL model reads

$$\mathcal{L}_{\rm NJL} = \bar{\psi}(i\gamma^\mu\partial_\mu - \hat{m}_0)\psi + \mathcal{L}_{\bar{q}q} + \mathcal{L}_{qq}, \tag{3}$$

where the chiral interaction part is

$$\mathcal{L}_{\bar{q}q} = G[(\bar{\psi}\psi)^2 + (\bar{\psi}i\gamma_5\vec{\tau}\psi)^2], \tag{4}$$

and the diquark part which is relevant to the mean-field condensate (i.e. the spin, flavor, and color are all antisymmetric) is

$$\mathcal{L}_{qq} = H[(\bar{\psi}C\gamma_5\tau_2\lambda_A\bar{\psi}^T)(\psi^T C\gamma_5\tau_2\lambda_A\psi)]. \tag{5}$$

Here, $C = i\gamma_0\gamma_2$ stands for the Dirac charge conjugation matrix, and G and H are the coupling constants for the mesonic and diquark channels. The current quark mass matrix is given by $\hat{m} = \mathrm{diag}(m_u, m_d)$ in two flavors and we shall work in the isospin symmetric limit with $m_u = m_d = m$. We note that λ_A's are the antisymmetric Gell-Mann matrices (i.e. A runs over 2, 5, 7 only) for the color SU(3) group and $\vec{\tau}$'s are the Pauli matrices in flavor space.

For simplicity, the coupling constant in the vector channel is set to zero in this paper. The effect of the electric-charge neutrality on the chiral phase transition, including the Polyakov loop dynamics and the nonzero vector interaction, will be reported in our future work [15].

It deserves noting here that the scalar four-fermion interaction $\mathcal{L}_{\bar{q}q}$ in general consists of two types of different interactions [13,14,16], that is,

$$\mathcal{L}_1 = G_1[(\bar{\psi}\psi)^2 + (\bar{\psi}\vec{\tau}\psi)^2 + (\bar{\psi}i\gamma_5\psi)^2 + (\bar{\psi}i\gamma_5\vec{\tau}\psi)^2], \tag{6}$$

$$\mathcal{L}_2 = G_2[(\bar{\psi}\psi)^2 - (\bar{\psi}\vec{\tau}\psi)^2 - (\bar{\psi}i\gamma_5\psi)^2 + (\bar{\psi}i\gamma_5\vec{\tau}\psi)^2]. \tag{7}$$

Both interaction terms have the symmetry of $\mathrm{SU(2)_L} \times \mathrm{SU(2)_R} \times \mathrm{U(1)}$, while the axial symmetry, $\mathrm{U_A(1)}$, remains

only in $\mathcal{L}_1$. The $U_A(1)$ breaking part $\mathcal{L}_2$ belongs to the instanton-induced (two-flavor 't Hooft) interaction. In the mean-field level the constituent quark masses in the presence of $\mathcal{L}_1$ and $\mathcal{L}_2$ are

$$\begin{aligned} M_u &= m - 4G_1\langle\bar{u}u\rangle - 4G_2\langle\bar{d}d\rangle, \\ M_d &= m - 4G_1\langle\bar{d}d\rangle - 4G_2\langle\bar{u}u\rangle. \end{aligned} \tag{8}$$

Therefore, in general, $M_u \neq M_d$ if there exists a chemical potential mismatch between u quarks and d quarks by μ_e and thus $\langle\bar{u}u\rangle \neq \langle\bar{d}d\rangle$. If we introduce a parameter α to relate G_1 and G_2 to G in a way that

$$G_1 = (1-\alpha)G, \qquad G_2 = \alpha G, \tag{9}$$

we notice that the standard Lagrangian (4) corresponds to the case of $\alpha = 0.5$. In such a case, as is clear from Eq. (8), the constituent mass of u quarks is always identical to that of d quarks regardless of a difference in μ_u and μ_d. Once we get ready to proceed to the numerical calculations, in Sec. II C, we will check the dependence on α in a simple case without diquark condensation. In any case, because this paper aims to illustrate a general feature in the phase structure, we shall stick to the simplest choice $\alpha = 0.5$ which makes no difference in the qualitative picture.

Then, there are four model parameters left; the current quark mass m of u and d quarks, the coupling constants G and H, and the three-momentum cutoff Λ. In this work, we take the same parameters as in Ref. [17] which are fixed so as to reproduce the three physical quantities in vacuum; the pion mass $m_\pi \approx 140$ MeV, the pion decay constant $f_\pi \approx 94$ MeV, and the chiral condensate $\langle\bar{u}u\rangle = \langle\bar{d}d\rangle \approx -(251\ \text{MeV})^3$ with

$$m = 5.5\ \text{MeV}, \qquad G = 5.04\ \text{GeV}^{-2}, \qquad \Lambda = 0.651\ \text{GeV}. \tag{10}$$

The corresponding constituent quark mass in vacuum is 325.5 MeV for this set of the model parameter. The standard value of the ratio H/G is $3/4 = 0.75$, which is deduced by the Fierz transformation from the local current-current interaction. In this paper, we rather treat this ratio as a free parameter and shall perform a systematic survey.

B. Thermodynamic potential with neutrality condition

In general, the quark chemical potential matrix $\hat{\mu}$ takes the form [18]

$$\hat{\mu} = \mu - \mu_e Q + \mu_3 T_3 + \mu_8 T_8, \tag{11}$$

where μ is the quark chemical potential (i.e. one-third of the baryon chemical potential), μ_e is the chemical potential associated with the (negative) electric charge, and μ_3 and μ_8 represent the color chemical potentials corresponding to the Cartan subalgebra in color SU(3) space. The explicit form of the electric-charge matrix is $Q = \mathrm{diag}(\frac{2}{3}, -\frac{1}{3})$ in flavor space, and the color charge matrices are $T_3 = \mathrm{diag}(\frac{1}{2}, -\frac{1}{2}, 0)$ and $T_8 = \mathrm{diag}(\frac{1}{3}, \frac{1}{3}, -\frac{2}{3})$ in color space. The chemical potentials for different quarks are listed below:

$$\begin{aligned} \mu_{ru} &= \mu - \tfrac{2}{3}\mu_e + \tfrac{1}{2}\mu_3 + \tfrac{1}{3}\mu_8, \\ \mu_{gu} &= \mu - \tfrac{2}{3}\mu_e - \tfrac{1}{2}\mu_3 + \tfrac{1}{3}\mu_8, \\ \mu_{rd} &= \mu + \tfrac{1}{3}\mu_e + \tfrac{1}{2}\mu_3 + \tfrac{1}{3}\mu_8, \\ \mu_{gd} &= \mu + \tfrac{1}{3}\mu_e - \tfrac{1}{2}\mu_3 + \tfrac{1}{3}\mu_8, \\ \mu_{bu} &= \mu - \tfrac{2}{3}\mu_e - \tfrac{2}{3}\mu_8, \\ \mu_{bd} &= \mu + \tfrac{1}{3}\mu_e - \tfrac{2}{3}\mu_8. \end{aligned} \tag{12}$$

The four-quark interactions develop a dynamical quark mass with nonzero chiral condensate as

$$M = m - \sigma = m - 2G\langle\bar{\psi}\psi\rangle, \tag{13}$$

while the diquark condensate Δ and antidiquark condensate Δ^* could appear at high enough baryon density. Here, we follow the common treatment for two-flavor CSC that the blue quarks do not take part in the Cooper pairing.

Using the standard bosonization technique, the mean-field thermodynamic potential in the NJL model with the diquark degrees of freedom as well as the electron contribution takes the following form:

$$\begin{aligned} \Omega = \frac{\sigma^2}{4G} + \frac{\Delta^2}{4H} - \frac{1}{12\pi^2}\left(\mu_e^4 + 2\pi^2T^2\mu_e^2 + \frac{7\pi^4}{15}T^4\right) \\ - T\sum_n \int \frac{d^3p}{(2\pi)^3}\,\mathrm{Tr}\ln\frac{S_{\mathrm{MF}}^{-1}(i\omega_n, \vec{p})}{T}, \end{aligned} \tag{14}$$

where the sum runs over the Matsubara frequency $\omega_n = (2n+1)\pi T$ and Tr is taken over color, flavor, and Dirac indices. The inverse quark propagator matrix including both the chiral and diquark condensates in the Nambu-Gor'kov formalism is then given by

$$S_{\mathrm{MF}}^{-1}(i\omega_n, \vec{p}) = \begin{pmatrix} [G_0^+]^{-1} & \Delta\gamma_5\tau_2\lambda_2 \\ -\Delta^*\gamma_5\tau_2\lambda_2 & [G_0^-]^{-1} \end{pmatrix}, \tag{15}$$

with

$$[G_0^\pm]^{-1} = \gamma_0(i\omega_n \pm \hat{\mu}) - \vec{\gamma}\cdot\vec{p} - \hat{m}. \tag{16}$$

Taking the Matsubara sum, we can express the thermodynamic potential as usual as

$$\begin{aligned} \Omega(\mu_e, \mu_3, \mu_8, \sigma, \Delta; \mu, T) = \frac{\sigma^2}{4G} + \frac{\Delta^2}{4H} - \frac{1}{12\pi^2} \\ \times\left(\mu_e^4 + 2\pi^2T^2\mu_e^2 + \frac{7\pi^4}{15}T^4\right) \\ - \sum_{i=1}^{12}\int\frac{d^3p}{(2\pi)^3}\{E_i + 2T\ln(1 \\ + e^{-E_i/T})\}, \end{aligned} \tag{17}$$

with the dispersion relations for six quasiparticles [that is,

2 flavors × 3 colors; the spin degeneracy is already taken into account in Eq. (17)] and 6 quasianti-particles. The unpaired blue quarks have the following four energy dispersion relations:

$$E_{bu} = E - \mu_{bu}, \qquad \bar{E}_{bu} = E + \mu_{bu}$$
$$E_{bd} = E - \mu_{bd}, \qquad \bar{E}_{bd} = E + \mu_{bd}, \tag{18}$$

with $E = \sqrt{\vec{p}^2 + M^2}$. In the *rd-gu* quark sector with pairing we can find the four dispersion relations,

$$E^{\pm}_{rd\text{-}gu} = E_\Delta \pm \tfrac{1}{2}(\mu_{rd} - \mu_{gu}) = E_\Delta \pm \tfrac{1}{2}(\mu_e + \mu_3),$$
$$\bar{E}^{\pm}_{rd\text{-}gu} = \bar{E}_\Delta \pm \tfrac{1}{2}(\mu_{rd} - \mu_{gu}) = \bar{E}_\Delta \pm \tfrac{1}{2}(\mu_e + \mu_3), \tag{19}$$

and the *ru-gd* sector has another four as

$$E^{\pm}_{\mathrm{ru\text{-}gd}} = E_\Delta \pm \tfrac{1}{2}(\mu_{ru} - \mu_{gd}) = E_\Delta \mp \tfrac{1}{2}(\mu_e - \mu_3),$$
$$\bar{E}^{\pm}_{\mathrm{ru\text{-}gd}} = \bar{E}_\Delta \pm \tfrac{1}{2}(\mu_{ru} - \mu_{gd}) = \bar{E}_\Delta \mp \tfrac{1}{2}(\mu_e - \mu_3), \tag{20}$$

where $E_\Delta = \sqrt{(E - \bar{\mu})^2 + \Delta^2}$ and $\bar{E}_\Delta = \sqrt{(E + \bar{\mu})^2 + \Delta^2}$. The average chemical potential is defined by

$$\bar{\mu} = \frac{\mu_{rd} + \mu_{gu}}{2} = \frac{\mu_{ru} + \mu_{gd}}{2} = \mu - \frac{\mu_e}{6} + \frac{\mu_8}{3}. \tag{21}$$

For the two-flavor CSC case, the color charge corresponding to the matrix T_3 is always zero since the color SU(2) symmetry is left unbroken for red and green quarks. That means $\mu_3 = 0$. In contrast to that in the NJL model, nontrivial coupling to the Polyakov loop might induce a nonzero μ_3 in the case of the Polyakov loop augmented NJL (PNJL) model [19,20], which is beyond the current scope.

Since we know that μ_8 is much smaller than μ_e [18,21] to neutralize two-flavor CSC matter, the positive $\mu_e/6$ is overwhelming in Eq. (21) so that we can neglect μ_8 in the numerical calculation. The average chemical potential then amounts to Eq. (2).

Minimizing the thermodynamic potential (17), we can solve the mean fields σ and Δ together with the chemical potential μ_e from

$$\frac{\partial\Omega}{\partial\sigma} = \frac{\partial\Omega}{\partial\Delta} = \frac{\partial\Omega}{\partial\mu_e} = 0. \tag{22}$$

C. Dependence on α and the constituent quark mass difference

For the cases with $\alpha \neq 0.5$, as we have mentioned, M_u should be different from M_d in the presence of nonzero μ_e, which is apparent in Eq. (8). Figure 1 shows the dependence on α in the behavior of M_u, M_d, and μ_e as a function of μ at a fixed temperature $T = 5$ MeV. We do not take account of the diquark condensate for the moment. From the figure we note the following two points: First, μ_e becomes larger with increasing α, and the first-order phase transition tends to occur at a higher chemical potential. This means that the value of μ_e, which plays a role similar to the vector interaction in the chiral phase transition, is sensitive to the magnitude of the flavor-mixing interaction. Second, in contrast to their absolute values of masses, we see that the mass differences between u and d quarks are sizable for $\alpha = 0$ and $\alpha = 0.1$, while the mass difference becomes minor for $\alpha \geq 0.2$.

It should be noted that the strength of the flavor-mixing interaction which originates from the $U_A(1)$ anomaly may be small in comparison with the $U(2) \times U(2)$ symmetric part, and it would be intriguing to explore its effect on M_u and M_d. We stress, however, that we should perform such studies for the three-flavor case where the quantitative effect of the $U_A(1)$ anomaly is more clearly seen in the η-η' system (for instance [22]). In the present two-flavor analysis, therefore, we shall only consider $\alpha = 0.5$ for elucidating the effect of μ_e on the chiral and CSC phase

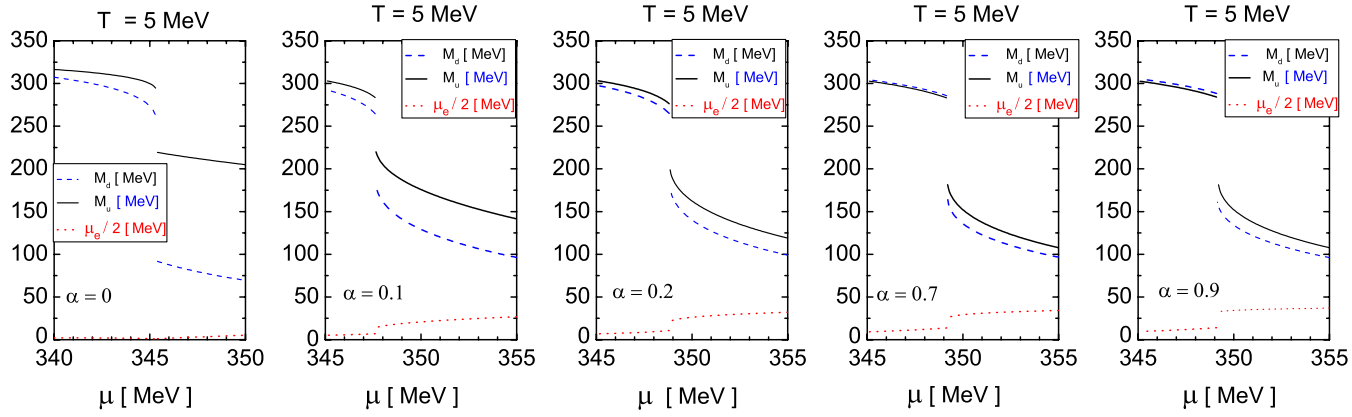

FIG. 1 (color online). The constituent quark mass difference between u and d quarks for $\alpha = 0$, 0.1, 0.2, 0.7, 0.9, where α is a parameter to indicate the flavor-mixing interaction defined in Eq. (9). All results are obtained under the electric charge neutrality and without diquark condensation.

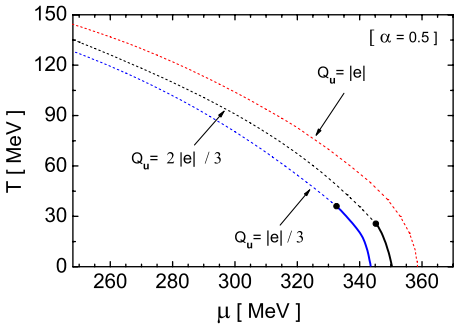

FIG. 2 (color online). The phase diagram for the chiral phase transition under the electric-charge neutrality. The solid line (dashed line) represents the first-order transition (smooth crossover) and the filled circle dot locates the QCD critical point.

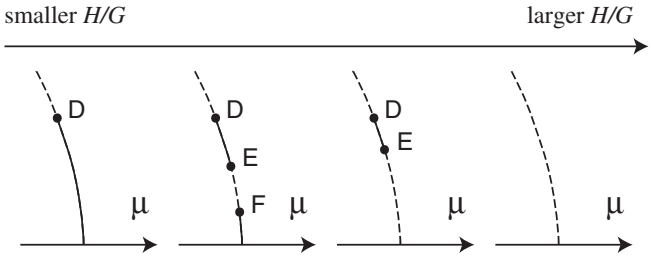

FIG. 3. The schematic change of the phase structure with increasing H/G from the left to the right. The solid and dashed lines represent the first-order transition and crossover, respectively. The number of the critical points depends on H/G.

transitions. Actually, Fig. 1 shows that we can reasonably ignore the difference between M_u and M_d induced by μ_e unless $\alpha < 0.2$.

It is known that as the coupling constant G_{V} of the vector interaction increases, the whole critical or crossover line of the chiral phase transition shifts toward larger chemical potential and the critical point moves toward smaller temperature and larger chemical potential, which disappears eventually at a large value of G_{V} [8–11]. Let us show that the μ_e affects the phase diagram in a similar way as G_{V}, which is anticipated from Eqs. (1) and (2). To demonstrate it clearly, we try to enhance the effect of μ_e artificially by varying the u-quark electric charge Q_u by hand as $Q_u = |e|, 2|e|/3, |e|/3$, while keeping the d quarks unchanged: The case of $Q_u = |e|/3$ corresponds to the situation with no net effect on the average chemical potential. The real world is $Q_u = 2|e|/3$. We can induce a further large net shift in the average chemical potential by taking $Q_u = |e|$. Figure 2 shows that the critical point shifts from $(T, \mu) = (36\ \mathrm{MeV}, 332\ \mathrm{MeV})$ for $Q_u = |e|/3$ to $(T, \mu) = (24\ \mathrm{MeV}, 345\ \mathrm{MeV})$ for $Q_u = 2|e|/3$, and eventually disappears from the phase diagram when we choose $Q_u = |e|$. These results are quite reminiscent of the effects of changing G_V discussed in the literature [8–11].

III. NUMERICAL RESULTS AND DISCUSSIONS

In this section, we shall discuss the effect of electric-charge neutrality in β equilibrium on the phase structure with the CSC phase as well as with the chiral transition taken into consideration. We shall show that the μ_e induced by the neutrality constraint gives rise to a phase structure with multiple critical points, and the number of the critical points can be zero, one, two, and three.

Before presenting our numerical results, we shall give an intuitive account of the mechanism which causes the phase diagram with multiple critical points. We depict a schematic sketch in Fig. 3 which is useful to explain what would be anticipated in advance. There is a terminal point of the first-order phase boundary, that is the QCD critical point located at D, as long as the coupling ratio H/G is small and hence the neutrality constraint is not significant. When the coupling ratio H/G becomes substantially large, the critical line of the first-order phase transition is breached by the induced μ_e in the CSC phase, and there appear two more edges in the critical line of the first-order transition; the new critical points are denoted as E and F. Here we notice that there exist three critical points as a whole. So to speak, the first-order line attached to F is a ''survivor'' transition that surpasses the diquark effect at sufficiently low temperature where the first-order chiral transition remains strong. The first-order line D-E is, on the other hand, to be regarded as a ''remnant'' where the diquark condensate almost melts and would hardly affect the chiral transition. For a larger H/G, the survivor may be gone and then the two critical points D and E are left on the phase diagram. If we further increase H/G, all the first-order transitions of chiral restoration and all the critical points are washed away eventually.

In the subsequent subsections we shall present numerical results and see that what is described above is actually the case. For convenience we shall adopt the same notations as those in Ref. [6] to distinguish the different regions on the T-μ phase diagram; NG, CSC, COE, and NOR refer to the hadronic (Nambu-Goldstone) phase with $\sigma \neq 0$ and $\Delta = 0$, the color-superconducting phase with $\Delta \neq 0$ and $\sigma = 0$, the coexisting phase with $\sigma \neq 0$ and $\Delta \neq 0$, and the normal phase with $\sigma = \Delta = 0$, respectively, though they have exact meaning only in the chiral limit. In fact, as seen from our results such as Figs. 5(b), 7(b), and 8, and so on, M stays $10 \sim 100$ MeV even in CSC but near COE.

A. The case of intermediate diquark coupling

We first consider the standard ratio $H/G = 0.75$, which is usually referred to as the ''intermediate'' diquark coupling strength. Two phase diagrams with and without the charge-neutrality constraint are presented in Fig. 4; henceforth, the thick solid curve, the dashed curve, and the thin solid curve in the T-μ plane stand for the critical lines of first-order phase transition, smooth crossover, and second-order phase transition, respectively. Since the magnitude of

μ_8 is very small [21], as we have mentioned, we ignore it in the numerical calculation. We have checked that nonzero μ_8 has only a minor effect on our main results.

Both panels in Fig. 4 show that all the four phases, i.e., NG, CSC, COE, and NOR are realized in the phase diagram. The upper triple point at which the NG, CSC, and NOR phases encounter happens to be the critical point D for the chiral-to-CSC phase transition.

Figure 4(a) shows that the chiral phase transition keeps of first order at low temperatures even with the emergence of a COE phase when the charge-neutrality condition is not imposed. We remark that similar phase diagrams were obtained in the previous works [8,24–26] without imposing the charge-neutrality constraint in the NJL model, the instanton-based models, and the random matrix model.

In contrast to Fig. 4(a), one finds an unconventional phase structure in Fig. 4(b) where the charge-neutrality constraint is imposed: The would-be critical line for the first-order transition is terminated at two points E and F, between which the phase transition becomes crossover from COE to CSC. Hence there exist three distinct critical points, D, E, and F, as a whole. Although a possible phase structure with *two* critical points was suggested previously [6,8], the present work is the first model study that shows possible existence of *three* critical points in the QCD phase diagram.

In addition to the appearance of the three-critical-point structure, the following points are notable in Fig. 4(b):

(i) The critical line for the first-order chiral phase transition in the low-temperature region is shifted considerably toward higher quark chemical potential. Furthermore, the critical point D is somewhat shifted to lower T and higher μ; $(T, \mu) =$ (42 MeV, 330 MeV) $\rightarrow$ (33 MeV, 341 MeV). These are to be understood as the same effect of μ_e as we mentioned in the explanation of Fig. 2.

(ii) The coexisting region is widened both in the T and μ directions. The lower triple point of NG, COE, and CSC, labeled as E′ in Fig. 4(a) and E in 4(b), moves toward higher T and μ; $(T, \mu) =$ (5 MeV, 333 MeV) $\rightarrow$ (25 MeV, 343 MeV).

It is not difficult to understand the emergence of a smooth crossover for the chiral phase transition in the low-temperature region of the phase diagram when the diquark pairing is taken into account. The positive μ_e first considerably reduces the discontinuity in the constituent quark mass at the first-order transition, and then the competition between the chiral and diquark condensates leads to the complete disappearance of the discontinuity. This situation is similar to what happens with the vector interaction as described in Ref. [8]; in Ref. [8], though the charge-neutrality condition is not imposed, a similar phase diagram to ours is obtained and the enlargement of the coexisting phase is attributed to the enhanced competition between the chiral and diquark condensations by the vector interaction.

Now let us discuss the mechanism for realizing the three-critical-point structure shown in Fig. 4. For this sake, we also show, in Fig. 5, the μ and T dependence of M, Δ, and μ_e in the upper and lower panels, respectively. We see the nature of the chiral phase transition from low to high temperatures in order.

(1) In the low-temperature region below the critical point F, we have a first-order transition from the COE to CSC phase, as shown in Fig. 4(b). This feature is also clearly exhibited in the first panel of Fig. 5(a) and the fourth panel in Fig. 5(b) both of which show discontinuous jumps in the physical quantities. This result can be interpreted as follows: in this low-temperature region, the chiral condensate even in the COE phase has a rather large value and dominates over the diquark condensate at present diquark coupling $H/G = 0.75$. We should notice that the diquark condensate smears the Fermi surface like at finite temperature, which in turn tends to make the chiral transition weak [8]. In short, the effect of the diquark condensate is not yet strong enough in this temperature region to convert the

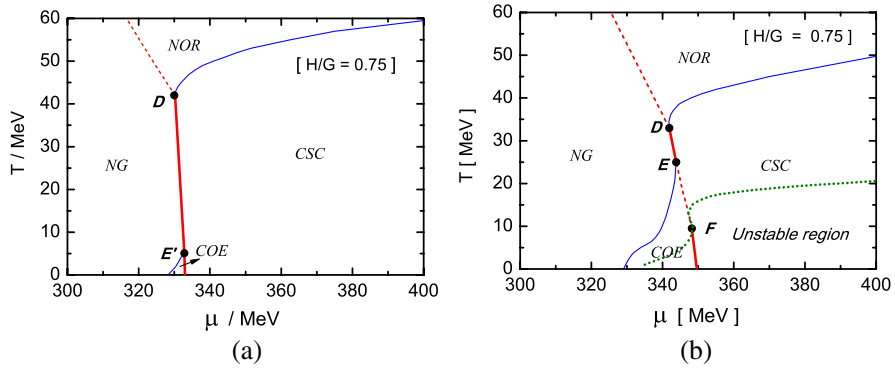

FIG. 4 (color online). The phase diagrams for the intermediate coupling constant $H/G = 0.75$, including the diquark condensate. The left (a) [right (b)] panel corresponds to the case without (with) enforcing the charge neutrality. In the left figure the unstable region is indicated by the dotted curve (see the discussion in Sec. III D).

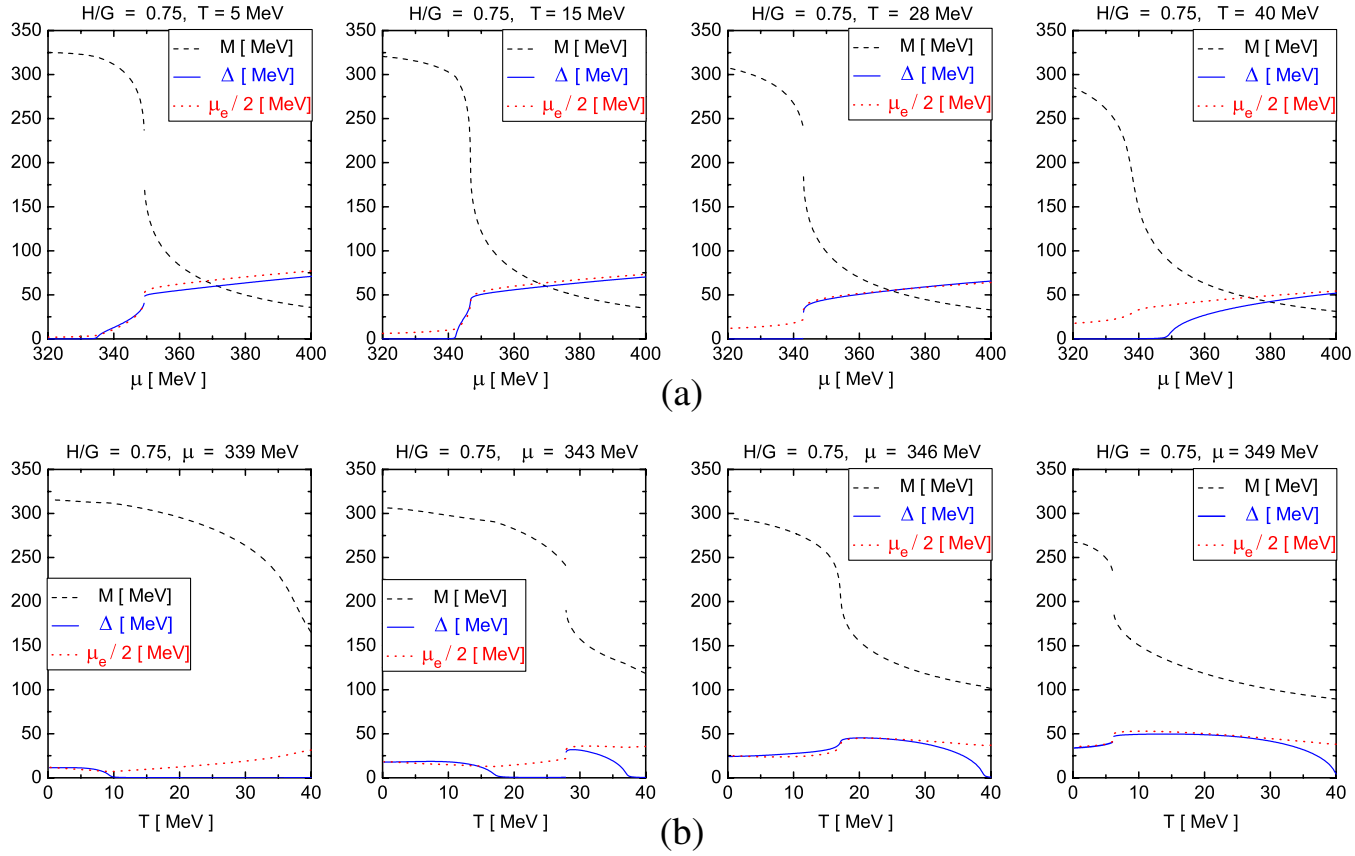

FIG. 5 (color online). M, Δ, and μ_e as functions of the chemical potential in (a) and the temperature in (b) for $H/G = 0.75$ under the condition of electric-charge neutrality.

first-order chiral phase transition to a smooth crossover. We identify this remaining first-order transition a survivor of the chiral transition which should be first order without the diquark condensate.

(2) Figure 4(b) shows that at intermediate temperatures between E and F, the chiral transition becomes smooth. The underlying mechanism for this may be understood from an unusual temperature dependence of the diquark condensate in the relevant chemical potential region. In fact, as shown in the third panel of Fig. 5(b), the diquark condensate increases as T is raised for a fixed μ. This is due to the combined effects of the charge-neutrality constraint and the temperature [21]: The neutrality constraint causes mismatched Fermi spheres for the quarks involved in the pairing, which unfavors the pairing, especially at small temperatures. At larger temperature, the mismatched Fermi surfaces are smeared enough to allow for the significant number of the quarks involved in the pairing, and hence the diquark condensate can develop. Besides, the chiral condensate decreases in a monotonic way with increasing temperature, and a smaller quark mass favors the formation of the diquark condensate because of a larger Fermi surface at a fixed μ. Thus the effect of the diquark condensate may overwhelm the chiral condensate at intermediate temperatures, which suppresses discontinuity in the chiral phase transition which turns to crossover.

(3) In the still higher temperature region, we find that the phase transition comes back to first order from NG to CSC, which is between D and E in Fig. 4(b). These features can be understood as follows. First, we note that D is attached to the critical line where Δ melts, and the diquark condensate decreases along D-E with the increasing temperature, as shown in the second panel of Fig. 4(b). It means that the chiral condensate dominates over the diquark pairing in this region. Thus the original feature of the chiral transition without the diquark condensation is intact there, and COE does not appear. We see that the chiral restoration remains of first order as shown in the third panel of Fig. 5(a) and the second panel of Fig. 5(b). In short, the first-order transition in this region is a remnant of the chiral restoration existing without the effect of the diquark pairing.

(4) For even higher temperatures than D, the chiral transition is a crossover and the condensates only show smooth behavior as seen in the fourth panel of Fig. 5(a) and the first panel in Fig. 5(b) where the

second-order nature of the CSC transition is also exhibited.

B. The case of strong diquark coupling

We next choose $H/G = 0.8$ and $H/G = 0.875$ as examples for the "strong" coupling case and present the corresponding phase diagrams in Fig. 6. One can see that, with increasing diquark coupling constant, the three-critical-point structure is first replaced by the two-critical-point structure and eventually the whole chiral phase transition becomes crossover. The phase boundary of the CSC phase is always a critical line of second-order transitions, which would be altered by gauge field fluctuations [27].

In contrast to Fig. 4(b), Fig. 6 shows that, as H/G increases, the critical lines for the chiral and diquark phase transitions shift toward the lower chemical potential direction and the COE region is relatively enlarged. This is a natural result since the enhanced diquark condensate more strongly suppresses the chiral condensate. It is interesting that the enhanced diquark condensate first converts the survivor line existing at intermediate coupling into crossover as noticed from Fig. 6(a) and then melts the remnant line down to crossover as shown in Fig. 6(b). This means that in the COE region the diquark condensate plays a dominant role over the chiral condensate and the original nature of the chiral transition fails to survive at low temperature. We remark that the two-critical-point structure in Fig. 6(a) is topologically the same as what was reported in Ref. [8], which may further illustrate an analogy between the positive μ_e and the repulsive vector interaction.

The dependence of M, Δ, and μ_e on μ (or T) for different fixed T (or μ) with $H/G = 0.8$ is presented in Fig. 7(a) (or 7(b)). All the figures show that all the physical quantities behave in accord with the above picture.

Figure 8 shows M, Δ, and μ_e as functions of T at four fixed chemical potentials at $H/G = 0.875$. We find that both the remnant and the survivor are breached by the large diquark condensate and no first-order transition remains. We only notice that Fig. 8 shows again the unusual temperature dependence of the diquark condensate, especially in the COE region; the diquark condensate is an increasing function of T in the low-temperature region, and then it decreases in the higher temperature region. The mechanism for this peculiar behavior of the diquark condensate has been accounted for in the last subsection. It is worthwhile to note that the fourth panels in Figs. 7(b) and 8 show that, if the diquark coupling is strong enough so that $\Delta \neq 0$ at $T = 0$, the nonmonotonous behavior of the gap energy exists no more, which only decreases with increasing temperature.

C. The case of weak diquark coupling

In this subsection, we present and discuss the phase diagrams for "weak" diquark coupling choosing $H/G = 0.7$ and 0.6875. As we will see, weakening the diquark coupling can lead to an unexpected complication in the phase diagram owing to the interplay between the chiral and diquark correlations, which is enhanced by the charge-neutrality constraint.

Figures 9(a) and 9(b) are the phase diagrams for $H/G = 0.7$ and 0.6875, respectively. Figure 9(a) shows that the smooth crossover line E-F seen in Fig. 4(b) shrinks in a way that the critical point F meets E at E′ on Fig. 9(a). Then, the three-critical-point structure is replaced by the usual one-critical-point structure. This is because the magnitude of the diquark condensate is too small to turn the chiral transition into crossover.

Let us briefly discuss a notable point that, for $H/G = 0.6875$, the critical point D and the triple point denoted by D′ can become separate. It seems that, as long as the diquark coupling is larger than a certain critical value, there is a mechanism to make D and D′ coincide. A similar observation is reported in the $2 + 1$ flavor case too [28]. If H/G is lowered further, our numerical calculation results in the shrinking COE and the enhancing (low-T) NOR regions.

Although we can recognize an intriguing structure in Fig. 9(b) in comparison to (a)—the emergence of a NOR "island" surrounded by the CSC phase at low T—we will not take a close look into this region. This is because the

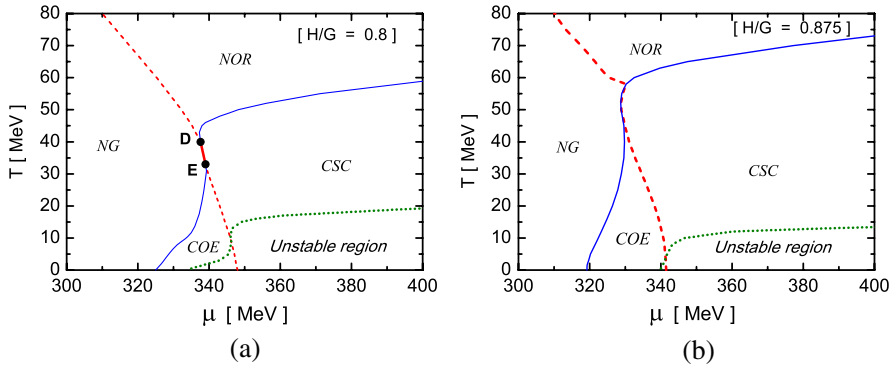

FIG. 6 (color online). The phase diagrams for the strong diquark couplings $H/G = 0.8$ (a) and $H/G = 0.875$ (b) under electric-charge neutrality. The unstable region is indicated by the dotted curve as previously.

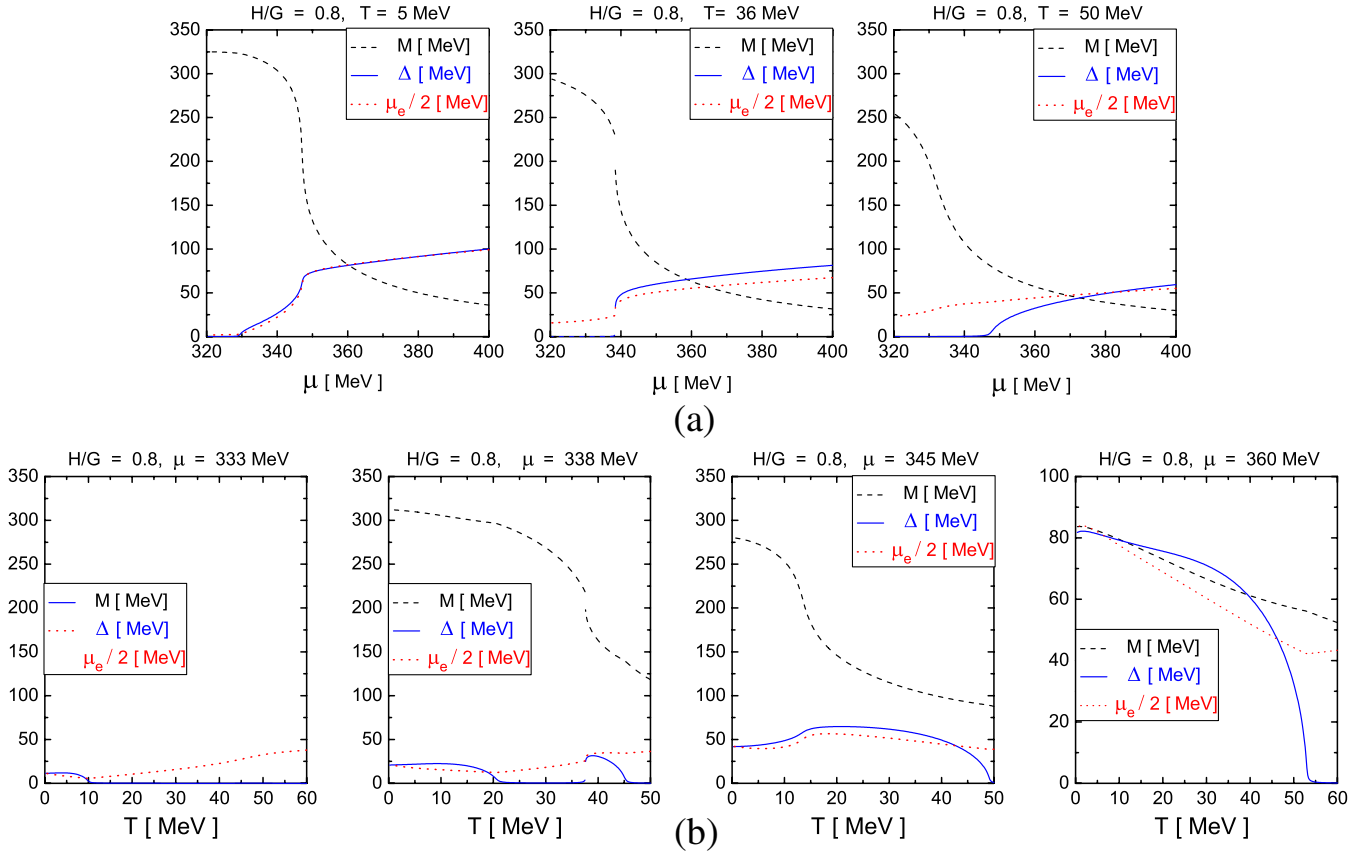

FIG. 7 (color online). M, Δ, and μ_e as functions of the chemical potential in (a) and the temperature in (b) for $H/G = 0.8$ under the condition of electric-charge neutrality.

newly arising NOR phase and the triple point G in Fig. 9(b) are located deeply in the unstable region, the boundary of which is indicated by the dotted curve. We shall address the instability problem in the next subsection.

D. Chromomagnetic instability

It has been known that the homogeneous CSC state could suffer from instability [29–33] when the Fermi surface mismatch grows comparable to the pairing gap. The instability occurs in various channels simultaneously [34], among which the transverse gluon field triggers the chromomagnetic instability. We can theoretically perceive the instability by the negative Meissner screening mass squared (or pure imaginary Meissner mass). In Figs. 4(b), 6, and 9 we have located the unstable region given by the condition that either of eight gluons has negative Meissner

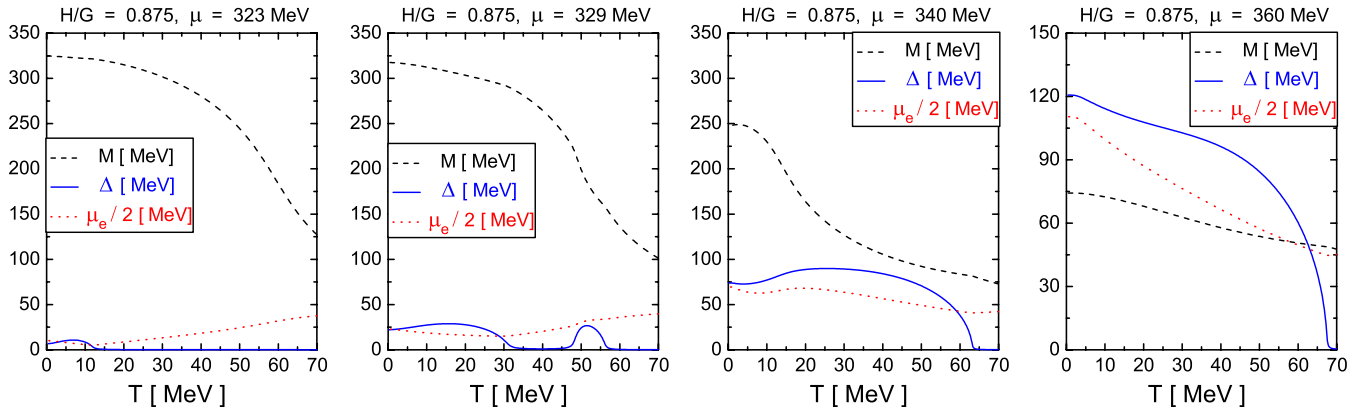

FIG. 8 (color online). M, Δ, and μ_e as functions of the temperature for $H/G = 0.875$ under the condition of electric-charge neutrality.

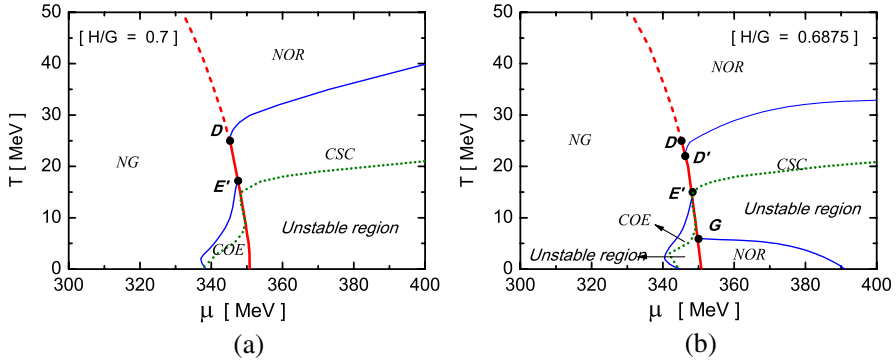

FIG. 9 (color online). The phase diagrams for the weak diquark couplings $H/G = 0.7$ and $H/G = 0.6875$ under electric-charge neutrality. The boundary of the unstable region is indicated by the dotted curve as previously.

mass squared. In what follows let us first explain how we calculate the Meissner mass.

In the two-flavor case the analytical expressions for the Meissner mass are available in the hard dense loop (HDL) approximation [29,35]. In our evaluation we have utilized them with our model parameters substituted to the formulae. We draw the dotted curves in Figs. 4(b), 6, and 9 in this way. At the same time we have carried out the brute-force computation by means of the potential curvature with respect to the gauge field source [33]. This calculation is necessary for the numerical check of the consistency between the HDL in Ref. [35] and the approximation made in this work. We have in fact confirmed the consistency in the case that we keep using a sharp three-momentum cutoff $\Lambda = 651$ MeV. It should be mentioned that how to renormalize the unphysical cutoff dependence is not yet known in a field-theory manner [30]. Our prescription is motivated in accord with the NJL model treatment, while a larger Λ would make the unstable regions smaller. In this sense, even though the dotted curves in Figs. 4(b), 6, and 9 might move downward, the cutoff dependence would not affect the stable regions above them.

We show the Meissner masses squared for the fourth and eighth gluons at $H/G = 0.75$ as functions of μ in Fig. 10. We note that the Meissner mass squared changes rapidly from NG to COE leading to the chromomagnetic instability in the high-μ and low-T region of COE and CSC as indicated by the dotted curve in Fig. 4(b).

Figures 4(b) and 6(a) tell us that two critical points associated with the D-E line are outside the unstable region. However, the instability analysis solely cannot tell the fate of another critical point F in reality. In fact, there are two possibilities to accommodate three critical points; one is that the unstable region may shrink to lower temperature if the cutoff is taken large and the other is that some other H/G value may push F up above the unstable region. The latter case can been confirmed in the current model study when H/G is located in a narrow region near but below 0.75. To settle the robustness of F, we have to go into the identification of the true ground state inside the unstable region.

There are some attempts to overcome the chromomagnetic instability. The instability has a favorite direction leading to the (colored) Larkin-Ovchinnikov-Fulde-Ferrell (LOFF) state [34,36,37] (or spontaneous current generation [38,39], which shares the same mathematical structure with the colored plane-wave LOFF description [40]). We note that the gluonic phase [41] with one gluon

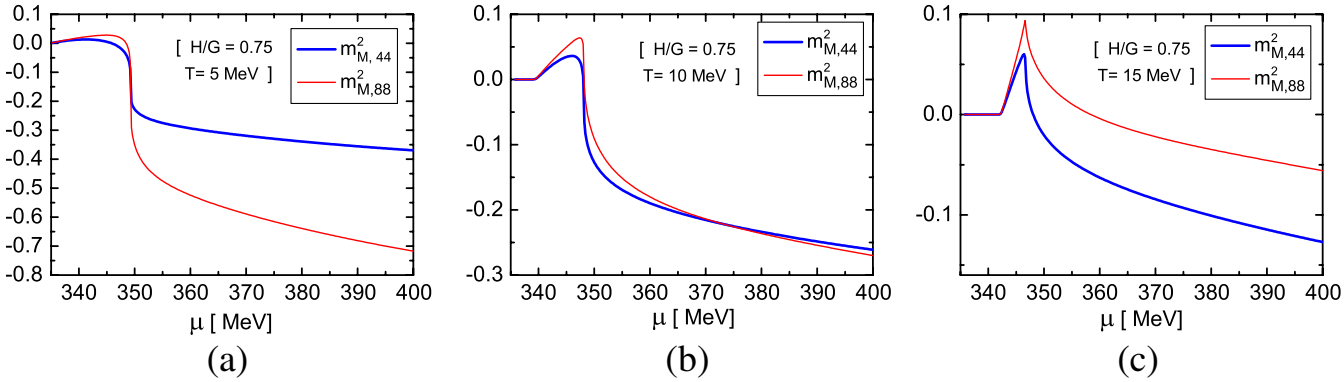

FIG. 10 (color online). Meissner masses squared as functions of μ for different temperatures with $H/G = 0.75$. All the results are in the unit $m_g^2 = 4\alpha_s^2\bar{\mu}^2/(3\pi)$.

condensate can translate into the plane-wave LOFF state, while a more stable gluonic phase with multiple gluon condensates has a chance to surpass the LOFF state [42]. The stable-unstable boundary we drew on the phase diagram can be regarded as a second-order phase transition line from the homogeneous CSC phase to one of these inhomogeneous states. Therefore, even though F in Fig. 4 (b) is overridden by the instability or the second-order phase transition, the physical consequence is very similar to the three-critical point structure, that is, one of the critical points is replaced by the critical line. Interestingly enough, then, Fig. 6(a) is indistinguishable from Fig. 4, meaning that the three-critical point (or line) interpretation is in effect elongated for a wider range of H/G due to the chromomagnetic instability.

E. Discussions

In the previous subsections, we have given a detailed account for four possible scenarios for the critical point structure with the influence of the diquark condensate under the electric-charge neutrality. For the model parameters adopted here, numerical calculations suggest that the three-critical-point structure of the phase diagram appears in the range $0.735 \lesssim H/G \lesssim 0.767$, while the two-critical-point structure in the range $0.767 \lesssim H/G \lesssim 0.82$. For the stronger coupling region $H/G \gtrsim 0.82$, the chiral phase transition remains crossover, while for the weaker coupling region $H/G \lesssim 0.735$, only one-critical-point structure appears.

We have checked that the region with multi-critical-point structure is slightly modified quantitatively when nonzero μ_8 is taken into account; the range $0.745 \lesssim H/G \lesssim 0.772$ corresponds to the three-critical-point structure and $0.772 \lesssim H/G \lesssim 0.80$ to the two-critical-point one. Thus we can conclude that our main results on the novel phase structures are not altered even when the color-charge neutrality is fully incorporated although the parameter range leading to the multi-critical-point structure may be somewhat narrowed.

It should be noted that the multi-critical-point structure was not pointed out in the previous works such as Ref. [28] where the electric neutrality and the dynamical quark mass were simultaneously considered for $2 + 1$ flavor quark matter. Since the strange quark mass is still as large as the quark chemical potential near the chiral phase transition, the u and d quarks should play the dominant role in the vicinity of this region. Then, what causes the difference in the phase diagram? We have found that the appearance of the multi-critical-point structure is sensitive to the value of the constituent quark mass in the vacuum. In the present study the vacuum constituent quark mass for light quarks is 325.5 MeV, while it is 400 MeV in Ref. [28]. Notice that the larger the constituent quark mass is, the smaller the Fermi sphere becomes, disfavoring the diquark pairing for a given μ. Therefore, in Ref. [28], the strong first-order chiral transition at low temperature is hardly affected by the diquark even with μ_e, which could make the chiral transition smooth. However, in turn, it suggests the possibility that the multi-critical-point structure may appear even with the large constituent quark mass adopted in Ref. [28] if the repulsive vector interaction is also included, which is rather close to the realistic situation.

IV. CONCLUSIONS AND OUTLOOK

In this paper, we have explored the effect of electric-charge neutrality in β equilibrium on the chiral phase transition with and without considering the diquark condensate within a simple two-flavor NJL model.

We first disclosed the similarity of the roles on the chiral phase transition played by the positive electric chemical potential and the repulsive vector interaction as follows: (1) Both of them make the chiral critical line at low temperature shift toward larger quark chemical potential and effectively weaken the first-order chiral phase transition. (2) Both of them effectively enhance the competition between the chiral and diquark condensates.

In some model parameter region, including the diquark condensate, the combination of these two properties can result in the emergence of the two-critical-point structure for the chiral phase transition in the electric-charge neutral case. It is noticeable that the magnitude of the repulsive vector interaction in Ref. [8] was an assumption although the existence itself of such an interaction has a generic foundation; on the other hand, the positive electric chemical potential in this paper is self-consistently determined by the physical requirement that the bulk matter must be under the charge-neutrality condition.

Besides two nontrivial effects mentioned above, our investigation also showed a quite unconventional three-critical-point structure for the chiral phase transition. This result is directly associated with the abnormal behavior that the diquark energy gap can increase with increasing temperature in the coexisting region for a certain range of T-μ and H/G, which is possible under the tangled influences of electric-charge neutrality and the interplay between the chiral and diquark condensates. To our knowledge, so far, this is the first case which concretely demonstrates the three-critical-point structure for the chiral phase transition. Although this result with three critical points could be sensitive to the model parameter choice, it definitely gives a hint that there may exist a possibility that the complexity in QCD allows for more complicated phase boundaries associated with the chiral phase transition. Moreover we have studied the chromomagnetic instability and found that the three-critical-point scenario may be taken over by the structure with two critical points and one critical line. Our result also has a meaningful implication for the study of phase transitions leading to a coexisting phase involving superconductivity in condensed matter physics when external conditions are enforced to the sys-

tem like the neutrality constraint causing the mismatched Fermi surfaces.

In view of the common effects on the chiral phase transition by the positive μ_e and the repulsive vector interaction G_V, it is natural to expect that the influences mentioned above will be greatly enhanced when these two aspects are considered simultaneously. It is expected that the three-critical-point structure may extend to a weaker coupling region in the presence of the vector interaction, although the number of the critical points might change in a different way from that depicted in Fig. 3 when the vector coupling is increased.

In addition, the confinement-deconfinement phase transition at finite temperature and density is still poorly understood inside the CSC phase, that is because of the lack of confinement in the NJL-type model. Recently the PNJL was proposed [43,44] and had been extensively used to study the thermal properties and the phase transition of QCD [17,19,20,45–51]. It is interesting to investigate whether the results obtained in this paper are also true when including the Polyakov loop dynamics. Practically, the PNJL model tends to push the location of the critical point up toward the higher temperature region. That means a detailed structure observed in this work could be magnified by the Polyakov loop. More details on these two issues will be reported in our future publication [15], and in fact, we have already verified that the multi-critical-point structure still exists when the Polyakov loop effect is taken into account.

ACKNOWLEDGMENTS

One of the authors Z. Zhang thanks the support of the Grants-in-aid provided by the Japan Society for the Promotion of Science (JSPS). This work was partially supported by a Grant-in-Aid for Scientific Research by the Ministry of Education, Culture, Sports, Science and Technology (MEXT) of Japan (No. 20540265, No. 20740134, No. 19.07797), by the Yukawa International Program for Quark-Hadron Sciences, and by the Grant-in-Aid for the global COE program ''The Next Generation of Physics, Spun from Universality and Emergence'' from MEXT.

[1] K. Rajagopal and F. Wilczek, arXiv:hep-ph/0011333.
[2] D. H. Rischke, Prog. Part. Nucl. Phys. **52**, 197 (2004).
[3] M. Buballa, Phys. Rep. **407**, 205 (2005).
[4] M. G. Alford, A. Schmitt, K. Rajagopal, and T. Schafer, Rev. Mod. Phys. **80**, 1455 (2008).
[5] M. G. Alford, K. Rajagopal, and F. Wilczek, Nucl. Phys. **B537**, 443 (1999).
[6] T. Hatsuda, M. Tachibana, N. Yamamoto, and G. Baym, Phys. Rev. Lett. **97**, 122001 (2006); Phys. Rev. D **76**, 074001 (2007).
[7] T. Schafer and F. Wilczek, Phys. Rev. Lett. **82**, 3956 (1999); M. G. Alford, J. Berges, and K. Rajagopal, Nucl. Phys. **B558**, 219 (1999).
[8] M. Kitazawa, T. Koide, T. Kunihiro, and Y. Nemoto, Prog. Theor. Phys. **108**, 929 (2002).
[9] M. Asakawa and K. Yazaki, Nucl. Phys. A **504**, 668 (1989).
[10] S. Klimt, M. Lutz, and W. Weise, Phys. Lett. B **249**, 386 (1990).
[11] M. Buballa, Nucl. Phys. **A611**, 393 (1996).
[12] J. B. Kogut, D. Toublan, and D. K. Sinclair, Nucl. Phys. **B642**, 181 (2002).
[13] S. P. Klevansky, Rev. Mod. Phys. **64**, 649 (1992).
[14] T. Hatsuda and T. Kunihiro, Phys. Rep. **247**, 221 (1994).
[15] Z. Zhang and T. Kunihiro (work in progress).
[16] T. Hatsuda and T. Kunihiro, Prog. Theor. Phys. **74**, 765 (1985).
[17] Z. Zhang and Y. X. Liu, Phys. Rev. C **75**, 064910 (2007).
[18] M. Alford and K. Rajagopal, J. High Energy Phys. 06 (2002) 031; A. W. Steiner, S. Reddy, and M. Prakash, Phys. Rev. D **66**, 094007 (2002).
[19] S. Roessner, C. Ratti, and W. Weise, Phys. Rev. D **75**, 034007 (2007).
[20] H. Abuki, M. Ciminale, R. Gatto, G. Nardulli, and M. Ruggieri, Phys. Rev. D **77**, 074018 (2008); H. Abuki, R. Anglani, R. Gatto, G. Nardulli, and M. Ruggieri, Phys. Rev. D **78**, 034034 (2008).
[21] M. Huang and I. Shovkovy, Phys. Lett. B **564**, 205 (2003); Nucl. Phys. **A729**, 835 (2003).
[22] When the diquark condensate and the charge-neutrality constraint are not taken into consideration, the $U_A(1)$ anomaly term as given by the t' Hooft determinantal interaction in the three-flavor case does not give rise to any difference between the constituent quark masses once the current quark masses are set equal, as shown in Ref. [23]; see also Ref. [14].
[23] T. Kunihiro, Phys. Lett. B **219**, 363 (1989).
[24] R. Rapp, T. Schafer, E. V. Shuryak, and M. Velkovsky, Ann. Phys. (N.Y.) **280**, 35 (2000).
[25] G. W. Carter and D. Diakonov, Phys. Rev. D **60**, 016004 (1999).
[26] B. Vanderheyden and A. D. Jackson, Phys. Rev. D **62**, 094010 (2000).
[27] T. Matsuura, K. Iida, T. Hatsuda, and G. Baym, Phys. Rev. D **69**, 074012 (2004); I. Giannakis, D. f. Hou, H. c. Ren, and D. H. Rischke, Phys. Rev. Lett. **93**, 232301 (2004).
[28] H. Abuki and T. Kunihiro, Nucl. Phys. **A768**, 118 (2006).
[29] M. Huang and I. A. Shovkovy, Phys. Rev. D **70**, 051501 (R) (2004); **70**, 094030 (2004).
[30] M. Alford and Q. h. Wang, J. Phys. G **31**, 719 (2005).
[31] R. Casalbuoni, R. Gatto, M. Mannarelli, G. Nardulli, and M. Ruggieri, Phys. Lett. B **605**, 362 (2005); **615**, 297(E)

(2005).
[32] K. Fukushima, Phys. Rev. D **72**, 074002 (2005).
[33] O. Kiriyama, Phys. Rev. D **74**, 114011 (2006).
[34] K. Iida and K. Fukushima, Phys. Rev. D **74**, 074020 (2006).
[35] L. He, M. Jin, and P. Zhuang, Phys. Rev. D **75**, 036003 (2007).
[36] I. Giannakis and H. C. Ren, Phys. Lett. B **611**, 137 (2005).
[37] K. Fukushima, Phys. Rev. D **73**, 094016 (2006).
[38] M. Huang, Phys. Rev. D **73**, 045007 (2006).
[39] T. Schafer, Phys. Rev. Lett. **96**, 012305 (2006).
[40] K. Fukushima, arXiv:hep-ph/0510299.
[41] E. V. Gorbar, M. Hashimoto, and V. A. Miransky, Phys. Lett. B **632**, 305 (2006); Phys. Rev. Lett. **96**, 022005 (2006); Phys. Rev. D **75**, 085012 (2007).
[42] O. Kiriyama, D. H. Rischke, and I. A. Shovkovy, Phys. Lett. B **643**, 331 (2006); M. Hashimoto and V. A. Miransky, Prog. Theor. Phys. **118**, 303 (2007).
[43] K. Fukushima, Phys. Lett. B **591**, 277 (2004).
[44] C. Ratti, M. A. Thaler, and W. Weise, Phys. Rev. D **73**, 014019 (2006); C. Ratti, S. Roessner, and W. Weise, Phys. Lett. B **649**, 57 (2007).
[45] E. Megias, E. Ruiz Arriola, and L. L. Salcedo, Phys. Rev. D **74**, 065005 (2006).
[46] S. K. Ghosh, T. K. Mukherjee, M. G. Mustafa, and R. Ray, Phys. Rev. D **73**, 114007 (2006); **77**, 094024 (2008).
[47] H. Hansen, W. M. Alberico, A. Beraudo, A. Molinari, M. Nardi, and C. Ratti, Phys. Rev. D **75**, 065004 (2007).
[48] C. Sasaki, B. Friman, and K. Redlich, Phys. Rev. D **75**, 074013 (2007).
[49] W. j. Fu, Z. Zhang, and Y. x. Liu, Phys. Rev. D **77**, 014006 (2008); M. Ciminale, R. Gatto, N. D. Ippolito, G. Nardulli, and M. Ruggieri, Phys. Rev. D **77**, 054023 (2008).
[50] K. Fukushima, Phys. Rev. D **77**, 114028 (2008).
[51] Y. Sakai, K. Kashiwa, H. Kouno, and M. Yahiro, Phys. Rev. D **77**, 051901 (2008); **78**, 036001 (2008).